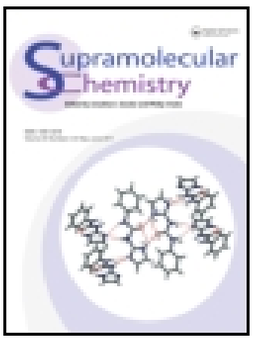

Supramolecular Chemistry

ISSN: 1061-0278 (Print) 1029-0478 (Online) Journal homepage: http://www.tandfonline.com/loi/gsch20

Indole-based distinctive chemosensors for 'naked-eye' detection of CN and HSO_4^-, associated with hydrogen-bonded complex and their DFT study

Dibyendu Sain, Chanda Kumari, Ashish Kumar & Swapan Dey

To cite this article: Dibyendu Sain, Chanda Kumari, Ashish Kumar & Swapan Dey (2015): Indole-based distinctive chemosensors for 'naked-eye' detection of CN and HSO_4^-, associated with hydrogen-bonded complex and their DFT study, Supramolecular Chemistry, DOI: 10.1080/10610278.2015.1092534

To link to this article: http://dx.doi.org/10.1080/10610278.2015.1092534

SUPRAMOLECULAR CHEMISTRY, 2015
http://dx.doi.org/10.1080/10610278.2015.1092534

Taylor & Francis
Taylor & Francis Group

Indole-based distinctive chemosensors for 'naked-eye' detection of CN^- and HSO_4^-, associated with hydrogen-bonded complex and their DFT study

Dibyendu Sain, Chanda Kumari, Ashish Kumar and Swapan Dey

Department of Applied Chemistry, Indian School of Mines, Dhanbad, India

ABSTRACT

Colorimetric detection of anions (**HSO_4^-** and **CN^-**) was achieved via analyte triggered colour changing of the dipodal and tripodal sensors in CH_3CN–H_2O (1:1). The sensors exhibited very sharp visual colour changes and fluorescence quenching–enhancing effect upon addition of the **HSO_4^-** and **CN^-**. The large downfield shift of the NH proton signals in ^{1}H-NMR complexation studies and quantum chemical DFT calculations proved the formation of hydrogen-bonded complexes where no proton transfer mechanism was found.

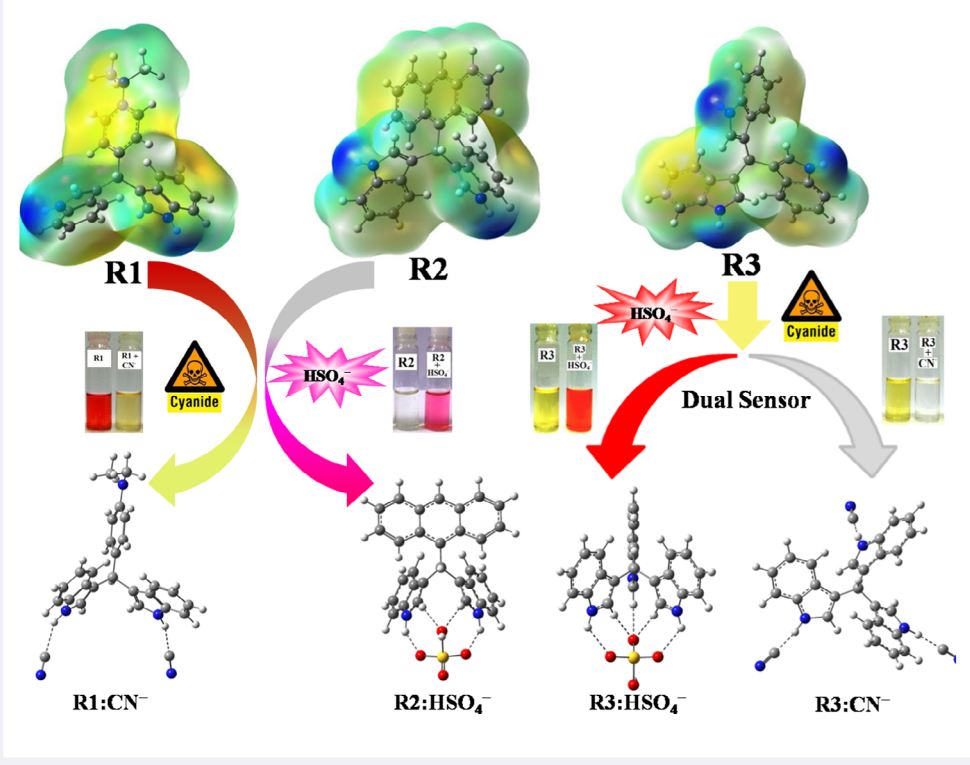

ARTICLE HISTORY
Received 3 June 2015
Accepted 6 September 2015

KEYWORDS
Dipodal and tripodal receptors; indole; chemosensors; **CN^-** and **HSO_4^-** ions

Introduction

The exposure on colorimetric sensors for identifying anions through hydrogen bonding interaction is an emerging research area (*1*). The anions have various fatal effects for human, mammals, aquatic life and the environment (*2*). The cyanide ion (**CN^-**) is considered as the most toxic ion for human body among all anions, as it binds Fe^{3+} of the *haem* unit and inhibits the oxygen supply in our body (*3*). Recently, limited numbers of fluorescent 'on-off' sensors (*4, 5*) and some reviews (*6*) have been focused for the detection of the **CN^-** ion through the hydrogen bonding interaction. Indeed, the development of easy and selective detectors for the cyanide ion is a great chance with simple chemosensors.

Selective detection and sensing of hydrogen sulfate (**HSO_4^-**) ion is an active research area as it is used in various fertilizers, industrial raw materials, nuclear fuel waste and it

CONTACT Swapan Dey dey.s.ac@ismdhanbad.ac.in

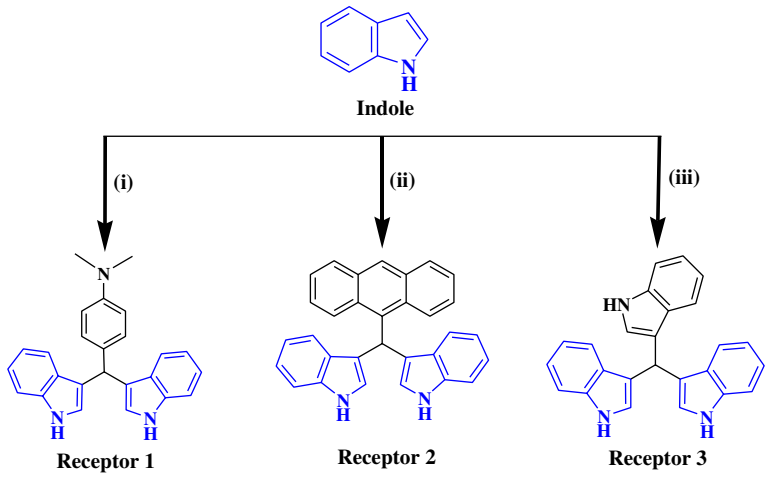

Scheme 1. (Colour online) *Reagents and conditions*: (i) *p-dimethylaminobenzaldehyde*, $Bi(NO_3)_3{\cdot}5H_2O$, dry ethanol, r.t., 6 h., 80% yield, (ii) *9-anthracenecarboxaldehyde*, $Bi(NO_3)_3{\cdot}5H_2O$, dry ethanol, r.t., 6 h., 85% yield, (iii) indole-3-carbaldehyde, $Bi(NO_3)_3{\cdot}5H_2O$, dry ethanol, r.t., 6 h., 90% yield.

also has a number of adverse effects as an environmental pollutant (*7*). At higher pH, the $\mathbf{HSO_4^-}$ ion dissociates to generate poisonous sulfate ion (SO_4^{2-}) which leads to diarrhoea, irritation of skin and eyes and respiratory paralysis (*8*). Till date, only a few fluorogenic chemosensors for sensing the $\mathbf{HSO_4^-}$ have been reported so far (*9*). So, the development of chemosensors for selective, '*naked-eye*' detection of the sulfate and hydrogen sulfate ions has attracted considerable attention as simple and cost-effective methods (*10*). Among the other techniques used for the detection of anions, fluorescence '*on-off*' technique has been fascinated much attention due to its high sensitivity (*11*).

In this present context, we report two indole-based dipodal (**R1** and **R2**) and one tripodal (**R3**) chemosensors for selective colorimetric sensing of $\mathbf{HSO_4^-}$ and $\mathbf{CN^-}$ ions in CH_3CN–H_2O (1:1). Herein, the indole moiety has been used as a binding site for the hydrogen bonding as well as a basic fluorophore unit (*12*). Earlier, Wei et al. have described the comparative study of anion sensing ability of the methyl substituted **R3**, where it did not show any spectral response to anions in CH_3CN only (*13*). However, in continuation of our research (*14*), we investigated the complexation studies for all the receptors in semi-aqueous medium (CH_3CN–H_2O, 1:1, v/v), where the receptors exhibit very sharp visual colour change and a fluorescence quenching–enhancing effect upon addition of $\mathbf{HSO_4^-}$ and $\mathbf{CN^-}$ selectively over other anions. Interestingly, no proton transfer incident from sensors to anions was observed under complexation but hydrogen-bonded complex formation was obviously established in ^{1}H-NMR study. Quantum chemical DFT calculations displayed the actual binding and interactions involved in the recognition process.

Reaction procedure for the synthesis of receptors (R1–R3)

R1 and **R2** were synthesised by the condensation reaction of indole with *N,N-dimethylaminobenzaldehyde* and *9-anthracenecarboxaldehyde*, respectively. The reactions were carried out in the presence of 0.1 equivalent bismuth nitrate pentahydrate as a catalyst in dry ethanol solvent. To prepare **R3**, the *indole-3-carbaldehyde* was first obtained from indole by Vilsmeier–Haack reaction using DMF and $POCl_3$ (*15*). Finally, the aldehyde was condensed with indole itself to produce **R3** (reaction Scheme 1).

Result and discussion

All the receptors (**R1**–**R3**) were characterised by FTIR, ^{1}H-NMR, ^{13}C-NMR and mass spectroscopic techniques. Only for **R3**, we obtained a single crystal to determine the geometry of the molecule in the solid state.

Single-crystal X-ray analysis of R3

The isothermal diffusion technique was followed to find out a good single crystal of **R3** using methanol (10%) in chloroform. The crystal was monoclinic in molecular setting with P 21/c space group and there were eight molecules present in a unit cell ($Z = 8$). The crystal structure of **R3** showed that the indole moieties were connected to the central sp^3 carbon (C1) atom to form a tripod structure, where the three N–H groups were far apart from each other (Figure 1(a)). In addition, one **R3** molecule was associated with the others by several short contacts in all directions to form a supramolecular network. The most important short contact was found among the NH

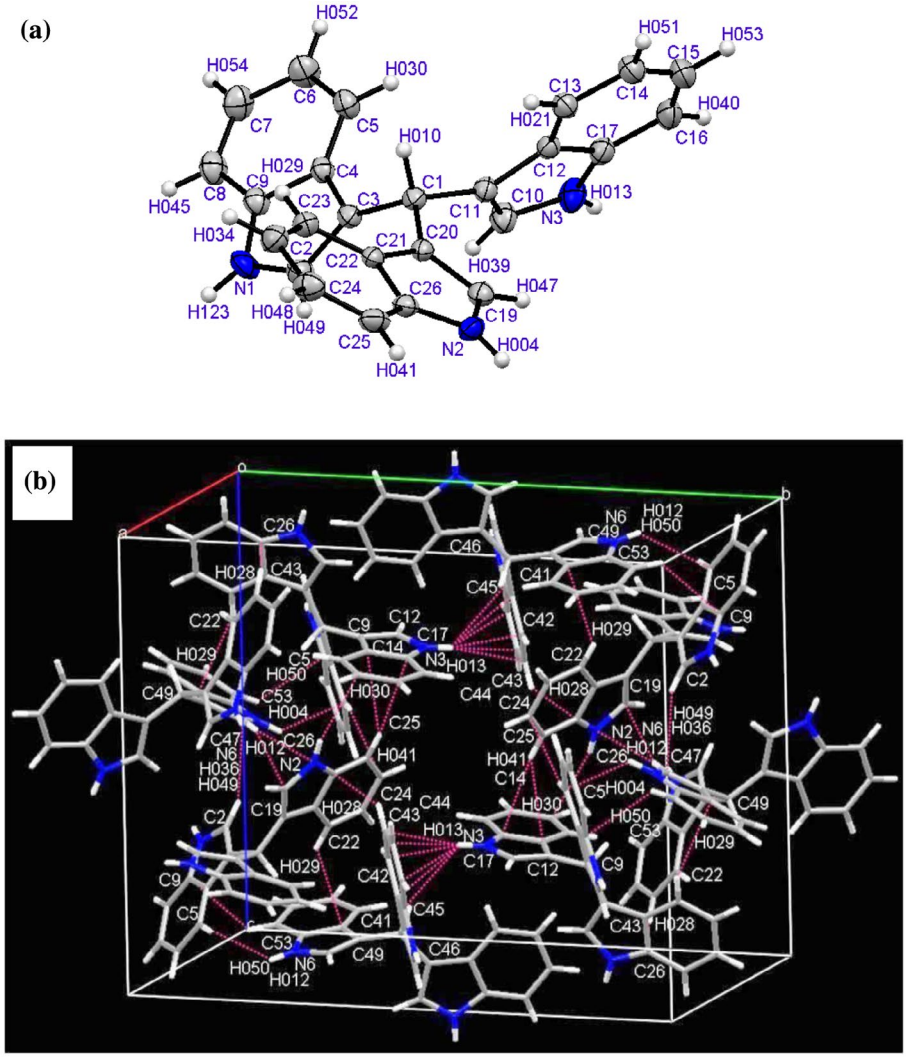

Figure 1. (Colour online) (a) ORTEP diagram of **R3** and (b) crystal packing diagram of **R3** in a unit cell (CCDC No. 868517).

group (N3–H013) and six aromatic carbon atoms (C41–C46) (Figure 1(b)). The different short contacts and the crystallographic data were summarised in Electronic Supplementary Information (ESI), Tables S1 and S2.

Complexation studies of the receptors with different anions through visual detection, UV–vis and fluorescence spectroscopy techniques

The sensing ability of the receptors was investigated with a series of anions ($[^nBu_4N]^+X^-$, X = F^-, Cl^-, Br^-, I^-, CN^-, AcO^-, HSO_4^- and $H_2PO_4^-$) in CH_3CN–H_2O (1:1, v/v). **R1** ($c = 1.09 \times 10^{-3}$ M) changed its colour from deep red to pale yellow only upon addition of 2.0 equivalent $\mathbf{CN^-}$ ion (Figure 2(a) inset), whereas **R2** ($c = 1.13 \times 10^{-3}$ M) turned to pink colour from colourless upon addition of 1.0 equivalent $\mathbf{HSO_4^-}$ (Figure 2(b) inset). On the other hand, **R3** ($c = 1.25 \times 10^{-3}$ M) instantly changed its colour (without taking time) from yellow to orange red (Figure 2(c) inset) upon addition of 1.0 equivalent $\mathbf{HSO_4^-}$ and consequently, became colourless by adding 3.0 equivalents $\mathbf{CN^-}$ ion (Figure 2(d) inset). However, the receptor solutions did not exhibit any interesting response by adding large amounts of other anions like F^-, Cl^-, Br^-, I^-, AcO^- and $H_2PO_4^-$ even up to 10.0 equivalents (see *ESI*, Figures S1, S6 and S10).

Absorption of **R1** ($c = 5.47 \times 10^{-4}$ M) was recorded using UV–vis spectroscopy and it showed two peaks at $\lambda_{max} = 535$ and 465 nm. It was also noticed that at lower concentration (2.52×10^{-5} M) an extra peak at $\lambda_{max} = 252$ nm was attributed to the indole ring with very high absorbance value (see *ESI*, Figure S2). The sharp decrease in absorbance was observed only by the addition of $\mathbf{\textit{n}Bu_4N^+CN^-}$ into the solution of **R1**. The absorbance at 535 nm decreased rapidly and the peak vanished finally, which resulted pale yellow (almost colourless) solution (Figure 2(a)). In case of **R2** ($c = 1.89 \times 10^{-4}$ M), it was seen that the receptor itself showed three absorption maxima at $\lambda_{max} = 352$, 370 and 391 nm. With the grad-

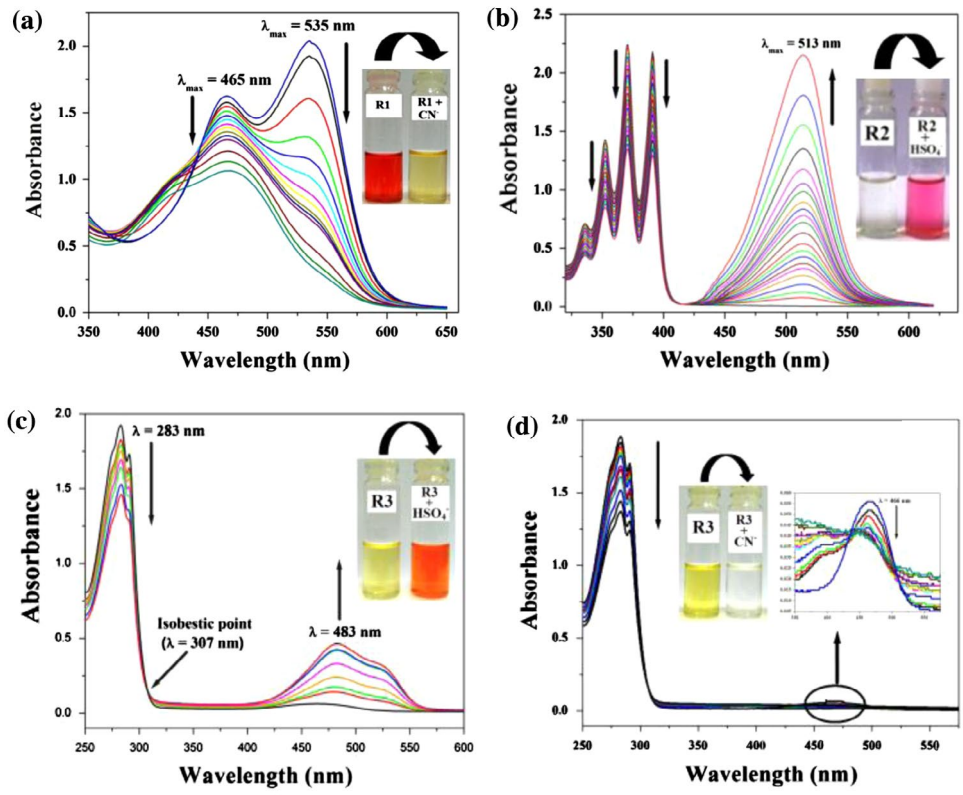

Figure 2. (Colour online) UV–vis titration spectra of (a) **R1** with CN^-, (b) **R2** with HSO_4^-, (c) **R3** with $\mathbf{HSO_4^-}$ and (d) **R3** with $\mathbf{CN^-}$ in $CH_3CN–H_2O$ (1:1, v/v) (Inset: visual colour change).

ual addition of $\mathbf{HSO_4^-}$ ion, the absorbance at 352, 370 and 391 nm decreased regularly along with an increase in a new absorption peak at λ_{max} = 513 nm (Figure 2(b)). This change was associated with the appearance of one isosbestic point at 420 nm, indicating the complex formation. On the other hand, **R3** ($c = 1.11 \times 10^{-4}$ M) itself exhibited an absorption maximum at λ_{max} = 283 nm, along with a secondary peak at 466 nm. In the presence of $\mathbf{HSO_4^-}$, the intensity of the absorbance at 283 nm decreased regularly along with increasing intensity of a new absorption band at λ_{max} = 483 nm (Figure 2(c)). The formation of one isosbestic point at 307 nm was found to support the complex formation. In contrast, the peak intensity at 466 nm decreased by the addition of $\mathbf{CN^-}$ to make **R3** solution colourless along with the regular decrease in intensity of the peak at 283 nm (Figure 2(d)). High polarisability over the H–N bonds of the receptors generated by the approach of the anions with the NH group of indole moieties through hydrogen bond formation. As a result, the energy of the benzene ring of the indole moiety moved to the N centres, which promoted the π-electron circulation in the indole moieties, causing considerable colour change and higher binding affinity for anions (*16*). The complexation process was occurring mainly due to hydrogen bond formation, not for deprotonation process. This phenomenon was also established by the anion sensing study of the receptor (**R3**) with strong base like tetrabutylammonium hydroxide. No colour change as well as λ_{max} shifting in UV–vis experiment was observed accordingly (see *ESI*, Figure S11).

For further investigation of solvatochromic effect, the UV–vis absorption study of **R3** was carried out in different solvents of different polarities, where it was observed that no characteristic peak was found in low polarity solvent like *n*-hexane and toluene (due to very low solubility) and the peak position of **R3** remained quite same (λ_{max} 274–283 nm) in high polarity solvent like DCM, chloroform, methanol, acetonitrile, DMF, DMSO and $CH_3CN–H_2O$ (1:1, v/v) (see *ESI*, Figure S12).

The complexation studies of the receptors with the anions were also carried out by the fluorescence spectroscopic analysis in $CH_3CN–H_2O$ (1:1, v/v). When **R1** (2.52×10^{-5} M) was excited at λ_{max} 252 nm, the corresponding emission spectrum was found at λ_{max} 360 nm. The regular decrease in the peak intensity, i.e. fluorescence quenching was observed upon addition of $\mathbf{CN^-}$ ion (Figure 3(a)). The calculated limit of detection (LOD) (*17*) of **R1** for sensing of $\mathbf{CN^-}$ was 2.03×10^{-8} M (see *ESI*). Corresponding emission peak of **R2** ($c = 1.42 \times 10^{-5}$ M) was found at 535 nm (λ_{exc} = 391 nm) with regular enhancement of the fluorescence intensity for $\mathbf{HSO_4^-}$ anion (0–3.0 equivalents) (Figure 3(b)) and **R2** can sense $\mathbf{HSO_4^-}$ up to the 1.98×10^{-8} M identified through LOD calculation. On exciting the solution

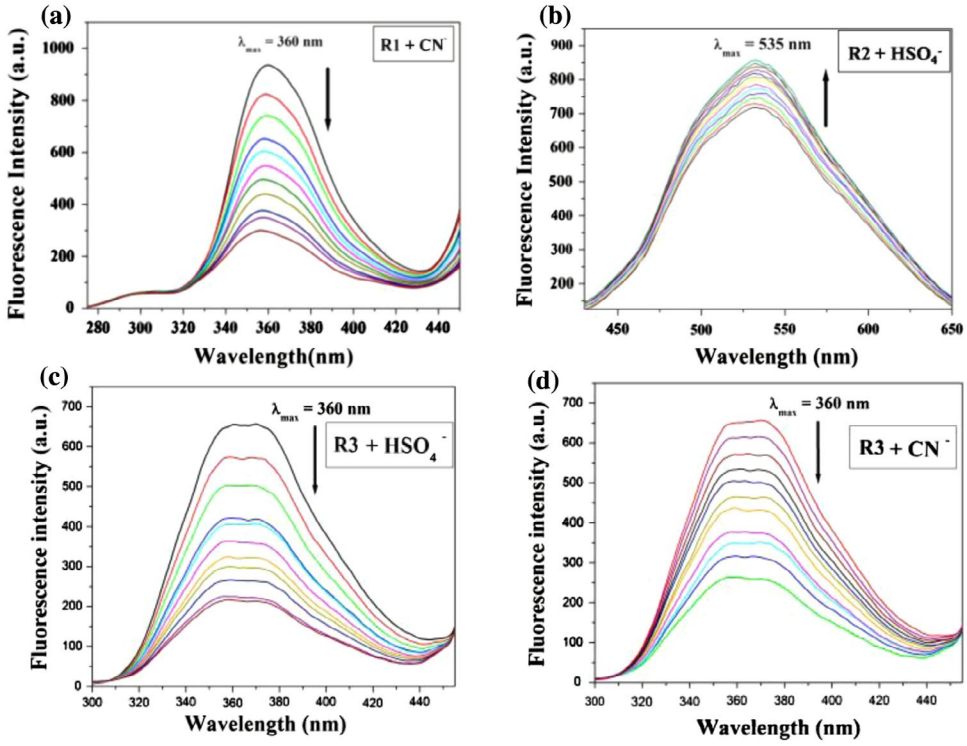

Figure 3. ((Colour online) a) Fluorescence titration spectra of (a) **R1** with $\mathbf{CN^-}$ (λ_{ex} = 252 nm), (b) **R2** with $\mathbf{HSO_4^-}$ (λ_{ex} = 391 nm), (c) **R3** with $\mathbf{HSO_4^-}$ (λ_{ex} = 283 nm) and (d) **R3** with $\mathbf{CN^-}$ (λ_{ex} = 283 nm) in CH_3CN–H_2O (1:1, v/v).

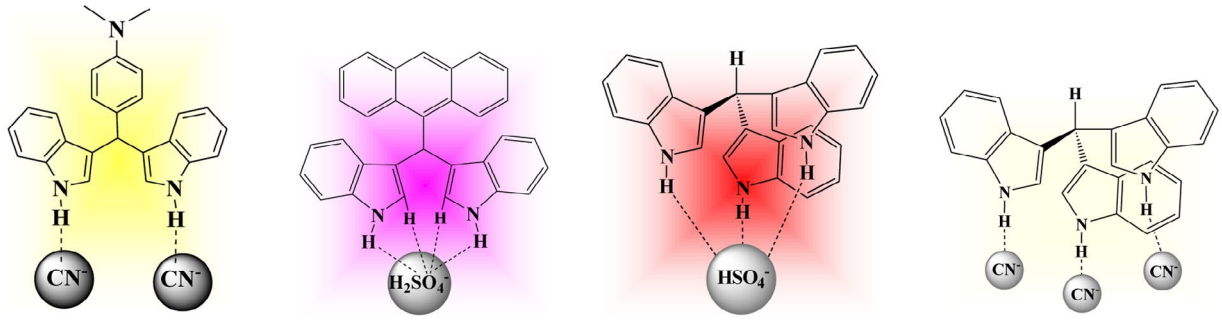

Figure 4. (Colour online) Probable complex structures of **R1**:$\mathbf{CN^-}$, **R2**:$\mathbf{HSO_4^-}$, **R3**:$\mathbf{HSO_4^-}$ and **R3**:$\mathbf{CN^-}$.

of **R3** ($c = 2.2 \times 10^{-6}$ M) at λ_{max} 283 nm, an emission spectrum with peak maxima at 360 nm was recorded and substantial quenching of the fluorescence intensity was observed with the gradual addition of both $\mathbf{HSO_4^-}$ and $\mathbf{CN^-}$ anion (0–3.0 equivalents, Figure 3(c) and (d)). The LOD calculation showed that **R3** recognise $\mathbf{HSO_4^-}$ and $\mathbf{CN^-}$ anions up to 2×10^{-8} M concentration (see *ESI*). Previously, a probable mechanism for the fluorescence quenching effect was reported by Mahapatra et al., which suggested an inversion between the strongly emissive $\pi\pi^*$ state and the poorly emissive $n\pi^*$ states of the fluorophore. Here, the complexation through the hydrogen bond formation of the indole NH group with the $\mathbf{HSO_4^-}$ and $\mathbf{CN^-}$ was responsible for the better stabilisation of n–π^* state compared to π–π^* state of the receptors, resulting a considerable decrease in the fluorescence emission intensity (*18*).

For the calculation of binding isotherm using UV–vis and fluorescence, the titration data were plotted as a function of [G]/[H] *vs* ΔI. It was observed that the curve after [G]/[H] = 2.0 tended to be parallel to *X*-axis and a break point of slope of the titration curve implied 1:2 stoichiometry between **R1** and $\mathbf{CN^-}$ (see *ESI*, Figure S3), whereas 1:1 stoichiometry was found for **R2** and **R3** with $\mathbf{HSO_4^-}$ (see *ESI*, Figures S7 and S13). The slope of the titration curve of **R3** with $\mathbf{CN^-}$ pointed out the breakpoint after [G]/[H] = 3, indicating 1:3 stoichiometry (see *ESI*, Figure S12). In addition, the Job's plot (*19*) (X_H *vs* Δ*I*. X_H, where X_H = mole fraction of the host, Δ*I* = Change in inten-

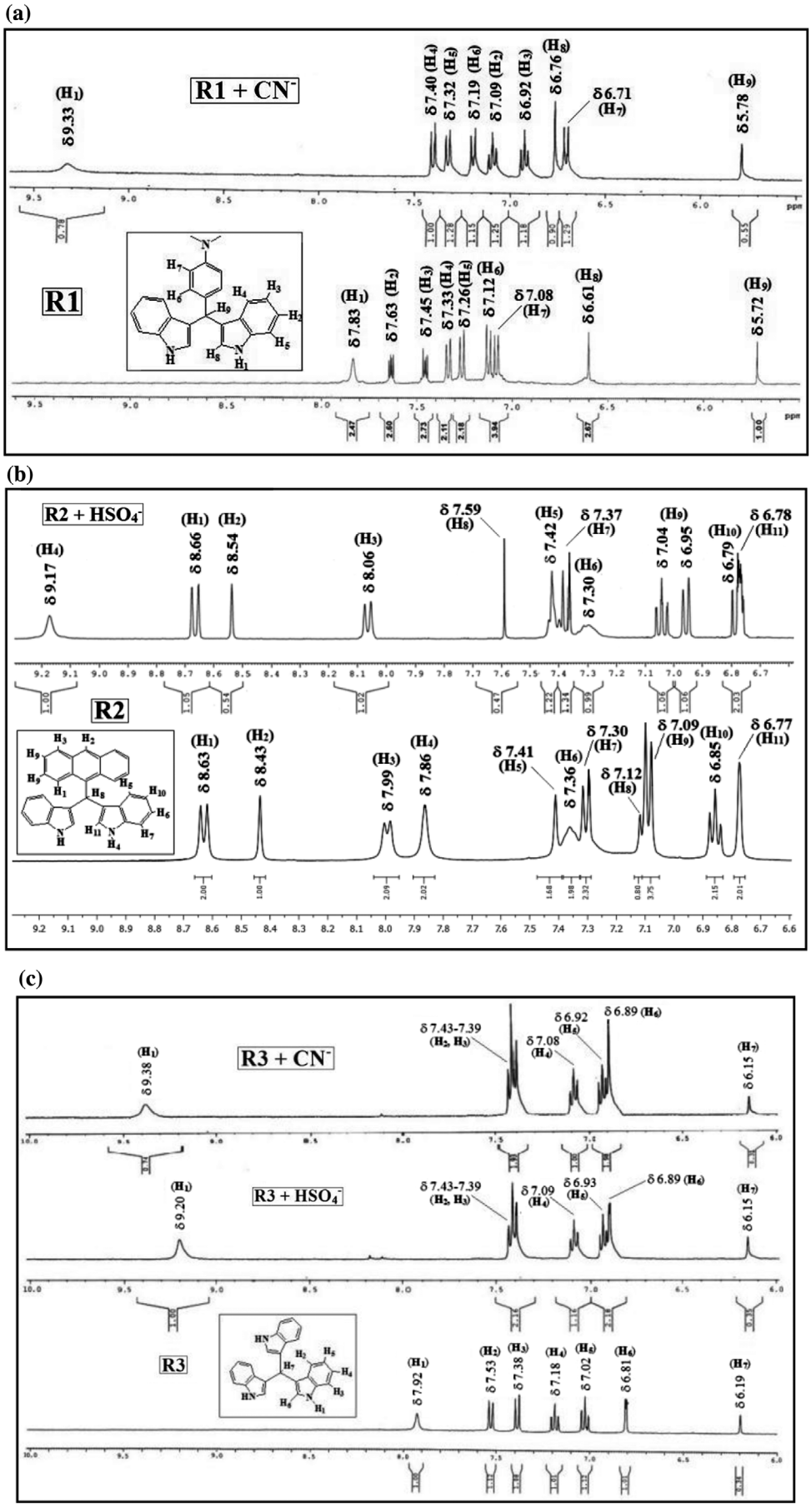

Figure 5. ^{1}H NMR spectra of (a) **R1** and **R1**:**CN**$^{-}$ complex (b) **R2** and **R2**:**HSO**$_4^{-}$ complex and (c) **R3**, **R3**:**HSO**$_4^{-}$ and **R3**:**CN**$^{-}$ in CD_3CN.

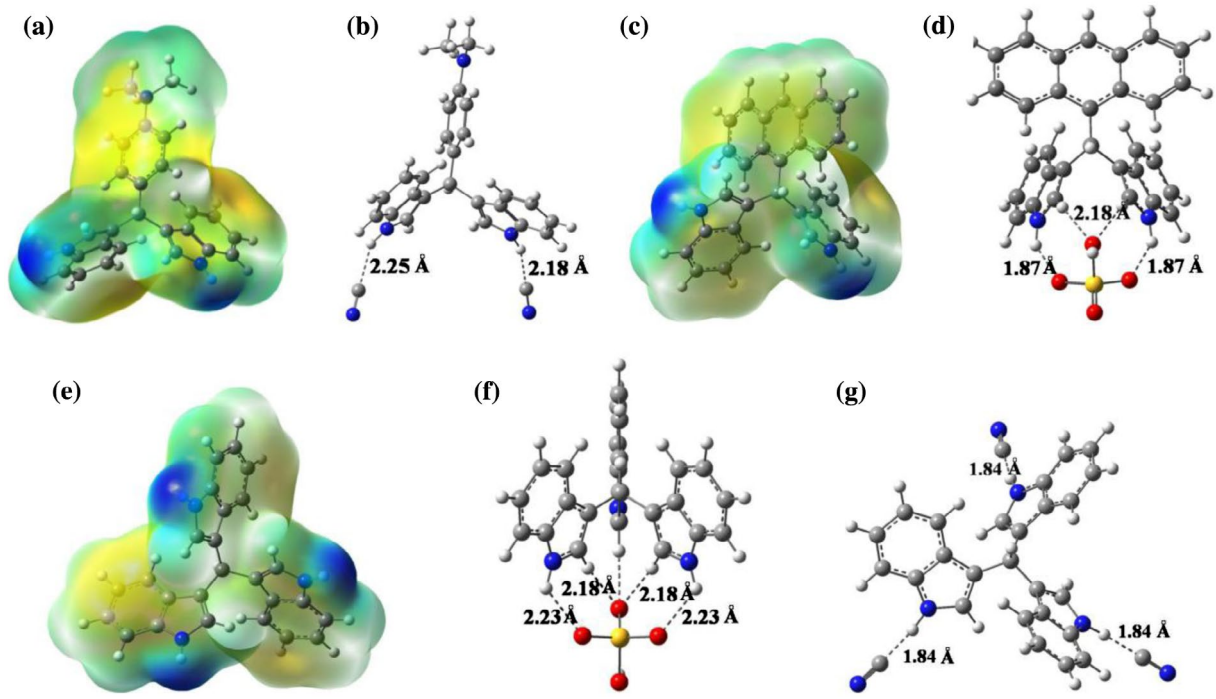

Figure 6. (Colour online) MEP map diagrams (positive regions in blue colour, isovalue for new surfaces: MO = 0.02, density = 0.0004) of (a) **R1**, (c) **R2**, (e) **R3**, and the optimised complex structures of (b) **R1**:$\mathbf{CN^-}$ complex, (d) **R2**:$\mathbf{HSO_4^-}$ complex, (f) **R3**:$\mathbf{HSO_4^-}$ complex and (g) **R3**:$\mathbf{CN^-}$ complex by DFT/B3LYP/6-31G method.

sity) in UV–vis and fluorescence titration also suggested the same stoichiometry of complexation (see *ESI*, Figure S14). The association constant (K_a) values of the receptors with all the anions were calculated by Benesi–Hildebrand linear plot (*20*) using UV–vis and fluorescence spectroscopic titration data. The highest association constant values were observed for **R1** with $\mathbf{CN^-}$, **R2** with $\mathbf{HSO_4^-}$ and **R3** with $\mathbf{HSO_4^-}$ and $\mathbf{CN^-}$ (see *ESI*, Tables S3, S4 and S5).

Complexation studies of the receptors using ^{1}H NMR technique

The specific complexation tendency of **R1** with $\mathbf{CN^-}$, **R2** with $\mathbf{HSO_4^-}$ and **R3** with $\mathbf{HSO_4^-}$ and $\mathbf{CN^-}$ were confirmed by the visual colour change, UV–vis and fluorescence experiments. Therefore, we performed the ^{1}H NMR complexation analysis of the receptors with the respective anions only. A probable binding mode of the respective complexes is presented in Figure 4.

From the ^{1}H NMR spectrum of **R1** in CD_3CN, it was clearly observed that the peak positions of **R1** shifted dramatically, when 2.0 equivalents ***n*Bu$_4$NCN** was introduced to **R1** solution (Figure 5(a)). The NH peak shifted from 7.83 to 9.33 ppm ($\Delta\delta$ 1.50 ppm) upon 1:2 complexation with $\mathbf{CN^-}$. Most of the aromatic protons of **R1** moved slightly up field, except the protons adjacent to NH groups (H_8) which shifted to a downfield region from 6.61 to 6.76 ppm ($\Delta\delta$ 0.15 ppm). The H_9 proton at the *meso* position appeared slightly down field upon complexation. In case of **R2**, the peak positions varied significantly with 1.0 equivalent $\mathbf{HSO_4^-}$ (Figure 5(b)) and the NH peak shifted from 7.86 to 9.17 ppm ($\Delta\delta$ 1.31 ppm) upon 1:1 complexation with $\mathbf{HSO_4^-}$. Most of the aromatic protons of **R2** appeared slightly down field. The proton at *meso* position shifted to downfield from 7.12 to 7.59 ppm ($\Delta\delta$ 0.47 ppm) upon complexation. While, the peak positions changed drastically for **R3** upon addition of 1.0 equivalent $\mathbf{HSO_4^-}$ and 3.0 equivalents $\mathbf{CN^-}$ ions (Figure 5(c)). The NH peak shifted from 7.92 to 9.20 ppm ($\Delta\delta$ 1.28 ppm) and 9.38 ppm ($\Delta\delta$ 1.46 ppm) on complexation with $\mathbf{HSO_4^-}$ and $\mathbf{CN^-}$, respectively. The aromatic protons of **R3** appeared slightly up field, except the protons adjacent to NH (H_6). The H_2 proton peak of **R3** merged with the peak of H_3 due to upfield shifting of H_2 (from 7.53 to 7.43 ppm, $\Delta\delta$ 0.10 ppm), which made the spectrum of the complexes broad in the aromatic region. Same peak broadening took place by merging two proton peaks (H_5 and H_6), where H_5 peak shifted to upfield (from 7.02 to 6.93 ppm, $\Delta\delta$ 0.09 ppm) and H_6 peak shifted to downfield (from 6.81 to 6.89 ppm, $\Delta\delta$ 0.08 ppm). The proton at meso position (H_7) moved to upfield slightly upon complexation. So, it could be summarised that the $\mathbf{CN^-}$ and $\mathbf{HSO_4^-}$ anions strongly coordinate with the NH groups of the respective receptors and drag the electron density from the neighbouring CH centres also.

Table 1. Energy of the receptors and their complexes with CN^- and HSO_4^-.

Receptors	R1	R2	R3	
Optimisation energy (a.u.)	−1130.83	−1304.14	−1128.09	
Complexes	R1:CN^-	R2:HSO_4^-	R3:HSO_4^-	R3:CN^-
Optimisation energy (a.u.)	−1316.59	−2003.07	−1827.42	−1406.47

Quantum chemical (DFT) calculation and molecular modelling studies

Quantum chemical DFT calculations were performed using *Gaussian09* (*21*) program package with the aid of the *GaussView 5.0* (*22*) visualisation program. The structure of the receptors and their complexes were optimised by density functional theory (DFT) in its restricted forms, using 6–31 g basis set and B3LYP procedure (*23*) DFT calculation and molecular modelling study exhibited the energy-optimised structures, electronic properties and the probable modes of binding through the formation of different hydrogen bonds between receptors and anions.

Molecular electrostatic potential (MEP) map diagram (Figure 6(a), (c), and (e)) displayed the most positive regions shown in deep blue colour and were sited mainly above the NH protons of indole moieties. The appearance of this positive region above the NH protons encouraged **CN^-** and **HSO_4^-** to take part for H-bonding. It was also found that the NH groups of each receptor (far apart from each other) could bind only larger size of anions which contained at least two available electrons donating centres for hydrogen bond formation. This criterion was perfectly fulfilled by the **HSO_4^-** anion due to the size and shape complementarity.

The optimised **R1:CN^-** complex structure suggested that **R1** could bind two **CN^-** ions individually as the 'NH' groups of **R1** remained far away from each other (Figure 6(b)). Due to the very high nucleophilic character of **CN^-**, it remained connected to the positive regions of **R1**, i.e. 'NH' centres through hydrogen bonding (2.25 and 2.18 Å). **R2:HSO_4^-** complex structure showed that two 'O' centres of **HSO_4^-** ion were connected through hydrogen bonding (1.87 Å) with the two N–H protons of **R2**. Two adjacent ring protons (C–H) of **R2** were also hydrogen bonded (2.18 Å) with another 'O' atom of **HSO_4^-** (Figure 6(d)). The complex structure of **R3** with **HSO_4^-** exhibited that the **HSO_4^-** ion was attached with **R3** in 1:1 fashion, where two NH protons of **R3** were connected with two 'O' atom of **HSO_4^-** individually through H-bonding interactions (2.23 Å). Another 'O' atom of **HSO_4^-** ion interacted with three adjacent C–H protons via three different hydrogen bonds (2.18 Å) formation (Figure 6(f)). On the other hand, **R3:CN^-** complex showed that three individual **CN^-** ions were connected to three different 'NH' centres of **R3** through hydrogen bonding (1.84 Å) (Figure 6(g)).

The electron density distribution of the receptors was distorted by the influence of the anions through the formation of different hydrogen bonds. So, the orbital diagrams of the highest occupied molecular orbital (HOMO) and the lowest unoccupied molecular orbital (LUMO) of the receptors and their complexes were investigated, which is shown in *ESI*, Figures S17, S18 and S19. Careful inspection of the MOs from DFT calculation shows that the position of HOMO or LUMO parts in the molecules is being changed upon complexation. Such different dispositions of the HOMO and LUMOs might be responsible for the visual colour change of the receptor solutions in the presence of anions. The quantum chemical DFT calculations also asserted the decrease in energy gap of HOMO and LUMO on complexation with **CN^-** and **HSO_4^-**, resulting the bathochromic shift in the UV–vis absorption spectra (*9g*) This calculation also pointed out the total energy of all the optimised complex structures were very low compare to the energy of their respective receptors (Table 1) and concluded the greater stability of the complexes than receptor itself.

Conclusions

In conclusion, we reported the design and synthesis of three indolyl dipodal and tripodal receptors (**R1**, **R2** and **R3**), which were very efficient colorimetric sensor for **CN^-** and **HSO_4^-** among other anions. **R1** showed strong binding interactions with highly poisonous cyanide (**CN^-**) ion, whereas **R2** exhibited very selective sensing ability towards toxic **HSO_4^-** ion. An interesting observation was found for **R3** as it could sense both **HSO_4^-** and **CN^-** selectively. The colour changes of the receptors in the presence of **CN^-** and **HSO_4^-** could be visualised instantly through naked eyes. UV–vis spectra, fluorescence spectra and ^{1}H-NMR spectra clearly pointed out the hydrogen-bonded complex formation of the receptors with the respective anions. Quantum chemical (DFT) calculations supported the above phenomena.

Experimental section

All reagents (AR grade) were purchased commercially and used without further purification. Solvents were dried following standard procedures. UV-grade CH_3CN was used for UV–vis and fluorescence titration. ^{1}H-NMR spectra were recorded on a Bruker AV400 instrument at 400 MHz with TMS as internal standard. ESI-MS measurements were carried out using a microTOF-Q II 10330 mass spectrometer. IR spectra were measured using Spectrum 2000 Perkin–Elmer Spectrometer. UV–vis spectra and fluorescence spectra were recorded using UV-1800 Shimadzu Spectrophotometer (1.0 cm quartz cell) and Perkin–Elmer LS 55 fluorescence spectrometer, respectively. Melting points were detected using Remco hot-coil stage melting point apparatus and are uncorrected.

Synthesis of 4-(di(1H-indol-3-yl)methyl)-N,N-dimethylbenzenamine (R1) (24)

Indole (0.393 g, 3.35 mmol) was mixed with 4-dimethylaminobenzaldehyde (0.25 g, 1.675 mmol) in dry ethanol (10.0 mL) followed by the addition of $Bi(NO_3)_3{\cdot}5H_2O$ (0.813 g, 0.167 mmol). After constant stirring at room temperature for 5 h, the reaction mixture was dried by removing ethanol and distilled water was added to get precipitate. The ppt. was then filtered and dried followed by the purification through column chromatography to obtain the desired pink colour receptor 1 (80% yield, m.p. 208–210 °C).

Spectral data of R1

^{1}H-NMR of R1 (400 MHz, CD_3CN): δ 7.83 (bs, 2H), 7.63 (q, J = 3.2 Hz, 2H), 7.45 (q, J = 3.2 Hz, 2H), 7.33 (d, J = 8.0 Hz, 2H), 7.26 (d, J = 8.4 Hz, 2H), 7.12 (d, J = 6.4 Hz, 2H), 7.08 (d, J = 6.4 Hz, 2H) 6.91 (s, 2H), 5.72 (s, 1H), 2.83 (s, 6H); **^{1}H-NMR of R1:CN^- complex (400 MHz, CD_3CN)**: δ 9.33 (bs, 2H), 7.40 (d, J = 8.0 Hz, 2H), 7.32 (d, J = 8.0 Hz, 2H), 7.19 (d, J = 8.0 Hz, 2H), 7.09 (t, J = 7.2 Hz, 2H), 6.92 (t, J = 7.2 Hz, 2H), 6.76 (s, 2H), 6.71 (d, J = 7.2 Hz, 2H), 5.78 (s, 1H), 2.88 (s, 6H); **^{13}C-NMR of R1 (100 MHz, $CDCl_3$)**: δ 149.0, 136.6, 129.2, 127.1, 123.4, 121.7, 120.4, 120.0, 119.0, 112.6, 112.1, 110.8, 40.8, 39.1, 29.6; **TOF-MS ES$^+$ (m/z, %)**: 367.06 (M+2, 20%), 366.05 (M+1, 100%), 364.04 (M−1, 30%); **FTIR (KBr, cm^{-1})**: 3405 (NH str.), 2926 (benzylic CH str.), 1726, 1604 (ar. C=C str.), 1515, 1111 (ar. C–N str.), 745 (NH bend.).

Synthesis of 3-((anthracen-9-yl)(1H-indol-3-yl)methyl)-1H-indole (R2) (25)

The condensation reaction between indole (227.5 mg, 1.94 mmole) and 9-anthracenecarboxaldehyde (200 mg, 0.97 mmole) was carried out in dry ethanol (10.0 mL) using $Bi(NO_3)_3{\cdot}5H_2O$ (94.2 mg, 0.19 mmole) as a catalyst with continuous stirring at room temperature for 6 h. After monitoring the completion of the reaction, ethanol was distilled off under vacuum. Distilled water was then added and the organic part was extracted with ethyl acetate for several times. The extracted organic part was now dried and purified through column chromatography using 20% Pet. Ether in $CHCl_3$ solvent to obtain pure receptor 2 (solid, off white colour, 85% yield, m.p. 240 °C).

Spectral data of R2

^{1}H NMR of R2 (400 MHz, CD_3CN): δ 8.63 (d, J = 9.2 Hz, 2H), 8.43 (s, 1H), 7.99 (d, J = 8.0 Hz, 2H), 7.86 (bs, 2H), 7.41 (s, 2H), 7.36 (bs, 2H), 7.30 (d, J = 8.0 Hz, 2H), 7.12 (s, 1H), 7.09 (d, J = 8.0 Hz, 4H), 6.85 (t, J = 7.6 Hz, 2H), 6.77 (s, 2H); **^{1}H NMR of R2:HSO_4^- complex (400 MHz, CD_3CN)**: δ 9.17 (bs, 2H), 8.66 (d, J = 9.2 Hz, 2H), 8.54 (s, 1H), 8.06 (d, J = 8.8 Hz, 2H), 7.59 (s, 1H), 7.42 (s, 2H), 7.37 (d, J = 8.0 Hz, 2H),7.30 (bs, 2H), 7.04 (t, J = 7.6 Hz, 2H), 6.95 (d, J = 8.0 Hz, 2H), 6.79 (s, 2H), 6.78 (m, 2H); **^{13}C-NMR of R2 (125 MHz, $CDCl_3$)**: δ 136.1, 134.7, 131.5, 128.7, 126.9, 126.8, 124.2, 123.5, 121.4, 119.6, 118.8, 118.5, 110.5, 34.6; **TOF-MS ES$^+$ (m/z, %)**: 423.1777 (M+1, 20%), 422.1728 (M^+, 40%), 421.1705 (M−1, 100%); **FTIR (KBr, cm^{-1})**: 3409 (NH str.), 3048 (benzylic CH str.), 1721, 1619 (ar C=C str.), 1454, 1417 (ar. C–N str.), 1338, 1092, 1014, 739 (NH bend.).

Synthesis of tri-(indol-3-yl)methane (R3) (26)

The condensation reaction between indole (807 mg, 6.89 mmol) and indole-3-carbaldehyde (500 mg, 3.445 mmol) was carried out in ethanol (10.0 mL) using $Bi(NO_3)_3{\cdot}5H_2O$ (167 mg, 0.344 mmol) as a catalyst with continuous stirring at room temperature for 6 h. After completion of the reaction, ethanol was distilled off under vacuum and distilled water was then added to precipitate the product. The residue was filtered, dried and purified through column chromatography using $CHCl_3$ solvent to obtain pure receptor 3 (solid, reddish brown colour, 90% yield, m.p. 235–237 °C).

Spectral data of R3

^{1}H NMR of R3 (400 MHz, CD_3CN): δ 7.92 (bs, 3H), 7.53 (d, J = 8.4 Hz, 3H), 7.38 (d, J = 8.0 Hz, 3H), 7.18 (t, J = 8.0 Hz, 3H), 7.02 (t, J = 7.6 Hz, 3H), 6.81 (s, 3H), 6.19 (s, 1H); **^{1}H NMR of R3:HSO_4^- complex (400 MHz, CD_3CN)**: δ 9.20 (bs, 3H), 7.43–7.39 (m, 6H), 7.09 (t, J = 7.6 Hz, 3H), 6.92 (t, J = 7.6 Hz, 3H), 6.89 (s, 3H), 6.15 (s, 1H); **^{1}H NMR of R3:CN^- complex (400 MHz, CD_3CN)**: δ 9.38 (bs, 3H), 7.43–7.39 (m, 6H), 7.08 (t, J = 8.0 Hz, 3H), 6.92 (t, J = 8.0 Hz, 3H), 6.89 (s, 3H), 6.15 (s, 1H); **^{13}C-NMR of R3 (100 MHz, $CDCl_3$)**: δ 136.6, 127.0, 123.3, 121.6, 120.0, 119.3, 118.9, 110.9, 29.6; **TOF-MS ES$^+$ (m/z, %)**: 385.01 (M+1+23, 30%), 384.01 (M+23, 100%), 360.02 (M−1, 25%), 245.03 (35%); **FTIR (KBr, cm^{-1})**: 3405 (NH str.), 3051 (benzylic CH Str.), 1609 (Ar. C=C str.), 1455, 1337 (Ar. C–N str.), 1089, 747 (NH def).

Acknowledgements

SD acknowledges Erasmus Mundus Action 2 AREAS+ for providing Postdoctoral fellowship. DS, CK and AK are sincerely thankful to Indian School of Mines for the Junior Research Fellowship. We are grateful to Professor Wim Dehaen, Department of Chemistry, KU Leuven for his valuable suggestion.

Supplemental material

Supplemental data for this article can be accessed here: http://dx.doi.org/10.1080/10610278.2015.1092536

References

(1) (a) Martinez-Manez, R.; Sancenon, F. *Chem. Rev.* 2003, *103*, 4419–4476; (b) Caltagirone, C.; Gale, P.A. *Chem. Soc. Rev.* 2009, *38*, 520–563; (c) Wiskur, S.L.; Ait-Haddou, H.; Lavigne, J.J.; Anslyn, E.V. *Acc. Chem. Res.* 2001, *34*, 963–972; (d) Amendola, V.; Fabbrizzi, L. *Chem. Commun.* 2009, 513–531.

(2) (a) Young, C.; Tidwell, L.; Anderson, C. *Cyanide Social, Industrial, and Economic Aspects*; Minerals, Metals, and Materials Society: Warrendale, PA, 2001; (b) Eisler, R. *Cyanide Hazards to Fish, Wildlife, and Invertebrates: A 80 Synoptic Review – U.S. Fish Wildl. Serv., Biol. Rep.* 1991, *85*, 1–58.

(3) (a) Baskin, S.I.; Brewer, T.G. In *Medical Aspects of Chemical and Biological Warfare: Cyanide Poisoning (Chapter 10)* Sidell, F.; Takafuji, E.T.; Franz, D.R. Eds.; TMM Publications: Washington, DC, 1997, *10*, 271–286; (b) Holland, M.A.; Kozlowski, L.M. *Clin. Pharm.* 1986, *5*, 737–741; (c) Way, J.L. *Annu. Rev. Pharmacol. Toxicol.* 1984, *24*, 451–481.

(4) (a) Kumar, S.; Singh, P.; Hundal, G.; Hundal, M.S.; Kumar, S. *Chem. Commun.* 2013, *49*, 2667–2669; (b) Mashraqui, S.H.; Betkar, R.; Chandiramani, M.; Estarellasb, C.; Fronterab, A. *New J. Chem.* 2011, *35*, 57–60; (c) Lee, K.S.; Kim, H.J.; Kim, G.H.; Shin, I.; Hong, J.I. *Org. Lett.* 2008, *10*, 49–51; (d) Li, M.-J.; Lin, Z.; Chen, X.; Chen, G. *Dalton Trans.* 2014, *43*, 11745–11751; (e) Wang, F.; Wang, L.; Chen, X.; Yoon, J. *Chem. Soc. Rev.* 2014, *43*, 4312–4324; (f) Garg, B.; Yan, L.; Bisht, T.; Zhu, C.; Ling, Y.-C. *RSC Adv.* 2014, *4*, 36344–36349; (g) Khairnar, N.; Tayade, K.; Bothra, S.; Sahoo, S.K.; Singh, J.; Singh, N.; Bendre, R.; Kuwar, A. *RSC Adv.* 2014, *4*, 41802–41806; (h) Wang, P.; Yao, Y.; Xue, M. *Chem. Commun.* 2014, *50*, 5064–5067; (i) Zhang, Y.; Yu, D.; Feng, G. *RSC Adv.* 2014, *4*, 14752–14757; (j) Peng, M.-J.; Guo, Y.; Yang, X.-F.; Suzenet, F.; Li, J.; Li, C.-W.; Duan, Y.-W. *RSC Adv.* 2014, *4*, 19077–19085.

(5) (a) Goswami, S.; Manna, A.; Paul, S.; Aich, K.; Das, A.K.; Chakraborty, S. *Tetrahedron Lett.* 2013, *54*, 1785–1789; (b) Saha, S.; Ghosh, A.; Mahato, P.; Mishra, S.; Mishra, S.K.; Suresh, E.; Das, S.; Das, A. *Org. Lett.* 2010, *12*, 3406–3409; (c) Hao, Y.; Chen, W.; Wang, L.; Zhou, B.; Zang, Q.; Chen, S.; Liu, Y.-N. *Anal. Methods* 2014, *6*, 2478–2483; (d) Lin, Y.-D.; Peng, Y.-S.; Su, W.; Tu, C.-H.; Sun, C.-H.; Chow, T.J. *Tetrahedron* 2012, *68*, 2523–2526; (e) Dong, Y.-M.; Peng, Y.; Dong, M.; Wang, Y.-W. *J. Org. Chem.* 2011, *76*, 6962–6966; (f) Xu, Z.; Chen, X.; Kim, H.N.; Yoon, J. *Chem. Soc. Rev.* 2010, *39*, 127–137; (g) Huh, J.O.; Do, Y.; Lee, M.H. *Organometallics* 2008, *27*, 1022–1025; (h) Konidena, R.K.; Thomas, K.R.J. *RSC Adv.* 2014, *4*, 22902–22910.

(6) (a) Xu, Z.; Chen, X.; Kim, H.N.; Yoon, J., *Chem. Soc. Rev.* 2010, 39, 127–137; (b) Kaur, K.; Saini, R.; Kumar, A.; Luxami, V.; Kaur, N.; Singh, P.; Kumar, S. *Coord. Chem. Rev.* 2012, *256*, 1992–2028.

(7) Moyer, B.A.; Delmau, L.H.; Fowler, C.J.; Ruas, A.; Bostick, D.A.; Sessler, J.L.; Katayeu, E.; Pantos, G.D.; Llinares, J.M.; Hossain, M.A.; Kang, S.O.; Bowman-James, K. *Supramolecular Chemistry of Environmentally Relevant Anions: Advances in Inorganic Chemistry* ed. Eldik, R.V.; Bowman-James, K., Academic Press: New York, 2006, *59*, 175–204.

(8) McKee, J.E.; Wolf, H.W. *Water Quality Criteria*, 2nd ed.; California State Water Quality Control Board: Sacramento, CA, 1963.

(9) (a) Goswami, S.; Das, S.; Aich, K.; Sarkar, D.; Mondal, T.K. *Tetrahedron Lett.* 2013, *54*, 6892–6896; (b) Bhardwaj, V.K.; Saluja, P.; Hundal, G.; Hundal, M.S.; Singh, N.; Jang, D.O. *Tetrahedron* 2013, *69*, 1606–1610; (c) Song, N.R.; Moon, J.H.; Choi, J.; Jun, E.J.; Kim, Y.; Kim, S.-J.; Lee, J.Y.; Yoon J. *Chem. Sci.* 2013, *4*, 1765–1771; (d) Kaur, P.; Kaur, H.; Singh, K. *Analyst* 2013, *138*, 425–428; (e) Yang, S.-T.; Liao, D.-J.; Chen, S.-J.; Hu, C.-H.; Wu, A.-T. *Analyst* 2012, *137*, 1553–1555; (f) Sarkar, D.; Pramanik, A.K.; Mondal, T.K. *RSC Adv.* 2014, *4*, 25341–25347; (g) Fegade, U.; Sahoo, S.K.; Singh, A.; Mahulikar, P.; Attarde, S.; Singh, N.; Kuwar, A. *RSC Adv.* 2014, *4*, 15288–15292; (h) Kumar, V.; Kumar, A.; Diwan, U.; Upadhyay, K.K. *Chem. Commun.* 2012, *48*, 9540–9542.

(10) (a) Ali, H.D.P.; Kruger, P.E.; Gunnlaugsson, T. *New J. Chem.* 2008, *32*, 1153–1161; (b) Lin, Z.H.; Ou, S.J.; Duan, C.Y.; Zhang, R.G.; Bai, Z.P. *Chem. Commun.* 2006, 624–626; (c) Hu, S.Z.; Guo, Y.; Xu, J.; Shao, S.J. *Org. Biomol. Chem.* 2008, *6*, 2071–2075; (d) Lopez, M.V.; Bermejo, M.R.; Vazquez, M.E.; Taglietti, A.; Zaragoza, G.; Pedrido, R.; Martinez-Calvo, M. *Org. Biomol. Chem.* 2010, *8*, 357–362.

(11) (a) Li, Q.; Guo, Y.; Shao, S. *Analyst* 2012, *137*, 4497–4501; (b) Hutt, J.T.; Jo, J.; Olasz, A.; Chen, C.-H.; Lee, D.; Aron, Z.D. *Org. Lett.* 2012, *14*, 3162–3165; (c) Gale, P.A.; Hiscock, J.R.; Lalaoui, N.; Light, M.E.; Wells, N.J.; Wenzel, M. *Org. Biomol. Chem.* 2012, *10*, 5909–5915; (d) Sakai, R.; Nagai, A.; Tago, Y.; Sato, S.; Nishimura, Y.; Arai, T.; Satoh, T.; Kakuchi, T. *Macromolecules* 2012, *45*, 4122–4127; (e) Fu, L.; Jiang, F.-L.; Fortin, D.; Harvey, P.D.; Liu, Y. *Chem. Commun.* 2011, *47*, 5503–5505.

(12) (a) Gale, P.A. *Chem. Commun.* 2008, 4525–4540; (b) Shiraishi, Y.; Maehara, H.; Hirai, T. *Org. Biomol. Chem.* 2009, *7*, 2072–2076; (c) Caltagirone, C.; Gale, P.A.; Hiscock, J.R.; Brooks, S.J.; Hursthouse, M.B.; Light, M.E. *Chem. Commun.* 2008, 3007–3009; (d) Dydio, P.; Zielinski, T.; Jurczak, J. *Chem. Commun.* 2009, 4560–4562.

(13) (a) Wang, L.; He, X.; Guo, Y.; Xu, J.; Shao, S. *Org. Biomol. Chem.* 2011, *9*, 752–757; (b) Wang, L.; Wei, W.; Guo, Y.; Xu, J.; Shao, S. *Spectrochim. Acta Part A* 2011, *78*, 726–731; (c) He, X.; Hu, S.; Liu, K.; Guo, Y.; Xu, J.; Shao, S. *Org. Lett.* 2006, *8*, 333–336; (d) Wei, W.; Guo, Y.; Xu, J.; Shao, S. *Spectrochim. Acta Part A* 2010, *77*, 620–624.

(14) (a) Dey, S.; Sain, D.; Goswami, S. *RSC Adv.* 2014, *4*, 428–433; (b) Dey, S.; Sain, D. *Supramol. Chem.* 2014, *26*, 769–776; (c) Dey, S.; Sain, D.; Kumar, A.; Kumari, C. *RSC Adv.* 2014, *4*, 51486–51495.

(15) (a) Mallegol, T.; Gmouh, S.; Meziane, M.A.A.; Blanchard-Desce, M.; Mongin, O. *SynthSIs* 2005, 1771–1774; (b) Fieser, L.F.; Hartwell, J.L.; Jones, J.E.; Wood, J.H.; Bost, R.W. *Org. Syn.* 1940, *20*, 11–13.

(16) (a) Hammud, H.H.; Ghannoum, A.; Masoud, M.S. *Spectrochim. Acta. Part A* 2006, *63*, 255–265; (b) Sain, D.; Kumari, C.; Kumar, A.; Dey, S. *Sens. Actuat. B* 2015, *221*, 849–856.

(17) (a) Shortreed, M.; Kopelman, R.; Kuhn, M.; Hoyland, B. *Anal. Chem.* 1996, *68*, 1414–1418; (b) Lin, W.; Yuan, L.; Cao, Z.; Feng, Y.; Long, L. *Chem. Eur. J.* 2009, *15*, 5096–5103; (c) Yang, Y.; Cheng, T.; Zhu, W.; Xu, Y.; Qian, X. *Org. Lett.* 2011, *13*, 264–267; (d) Zhu, M.; Yuan, M.; Liu, X.; Xu, J.; Lv, J.; Huang, C.; Liu, H.; Li, Y.; Wang, S.; Zhu, D. *Org. Lett.* 2008, *10*, 1481–1484.

(18) (a) Mahapatra, A.K.; Hazra, G.; Sahoo, P. *Beilstein J. Org. Chem.* 2010, *6*, 1–8; (b) Bazzicalupi, C.; Bencini, A.; Bianchi, A.; Borsari, L.; Danesi, A.; Giorgi, C.; Lodeiro, C.; Mariani, P.; Pina, F.; Santarelli, S.; Tamayo, A.; Valtancoli, B. *Dalton Trans.* 2006, 4000-4010.

(19) Job, P. *Ann. Chim.* 1928, *9*, 113–203.

(20) (a) Benesi, H.A.; Hildebrand, J.H. *J. Am. Chem. Soc.* 1949, *71*, 2703–2707; (b) Liao, J.-H.; Chen, C.-T.; Chou, H.-C.; Cheng, C.-C.; Chou, P.-T.; Fang, J.-M.; Slanina, Z.; Chow, T.J. *Org. Lett.* 2002, *4*, 3107–3110.

(21) Frisch, M.J., et al. *GAUSSIAN 09, Rev. D.01*; Gaussian, Inc.: Wallingford, CT, 2009.

(22) Dennington, R.D. (II), Keith, T.A.; Millam, J.M. *GaussView 5.0*, Gaussian, Inc.: Wallingford, CT, 2009.

(23) (a) Becke, A.D. *J. Chem. Phys.* 1993, *98*, 5648–5652; (b) Lee, C.; Yang, W.; Parr, R.G. *Phys. Rev. B* 1988, *37*, 785–789; (c) Becke, A.D. *Phys. Rev. A* 1988, *38*, 3098–3100.

(24) Gu, R.; Van Snick, S.V.; Robeyns, K.; Van Meervelt, L.V.; Dehaen, W. *Org. Biomol. Chem.* 2009, *7*, 380–385.

(25) Vahdat, S.M.; Khaksar, S.; Baghery, S. *Lett. Org. Chem.* 2012, *9*, 138–144.

(26) Deb, M.L.; Baruah, B.; Bhuyan, P.J. *Synthesis* 2008, 286–292.